Archives of Materials Science and Engineering

Volume 43
Issue 2
June 2010
Pages 77-86

International Scientific Journal
published monthly by the
World Academy of Materials
and Manufacturing Engineering

Torsional fatigue behaviour and damage mechanisms in the very high cycle regime

E. Bayraktar [a, b,*], H. Xue [c], F. Ayari [a, d], C. Bathias [b]

[a] Supmeca/LISMMA-Paris, School of Mechanical and Manufacturing Engineering, France
[b] CNAM- Arts & Métiers, Paris, Chair of Industrial materials laboratory, case 321, France
[c] North western Polytechnical University, School of Aircraft Design Engineering, Xi'an, China
[d] Laboratory of Mechanics, College of Science and Technology, 1008 Montfleury, Tunisia
* Corresponding author: E-mail address: bayraktar@supmeca.fr

Received 05.03.2010; published in revised form 01.06.2010

ABSTRACT

Purpose: of this paper: Many engineering components operate under combined torsion and axial cyclic loading conditions, which can result in fatigue fracture after a very long life regime of fatigue. This fatigue regime were carried out beyond 10^9 loading cycles called very high cycle fatigue (VHCF) to understand the fatigue properties and damage mechanisms of materials.

Design/methodology/approach: Torsional fatigue tests were conducted using a 20 kHz frequency ultrasonic fatigue testing device. The results obtained were compared to those of the conventional torsional fatigue test machine operated at 35 Hz to observe any discrepancy in results due to frequency effects between two experiments.

Findings: All the fatigue tests were done up to 10^{10} cycles at room temperature. Damage mechanisms in torsional fatigues such as crack initiation and propagation in different modes were studied by imaging the samples in a Scanning Electron Microscope (SEM). The results of the two kinds of material show that the stress vs. number of cycle curves (S-N curves) display a considerable decrease in fatigue strength beyond 10^7 cycles.

Research limitations/implications: Each test, the strain of specimen in the gage length must be calibrated with a strain gage bonded to the gage section. This is a critical point of this study. The results are very sensitive to the calibration system. Control of the displacement and the output of the power supply are made continuously by computer and recorded the magnitude of the strain in the specimen.

Practical implications: torsional fatigue tests has been investigated in the very high cycle fatigue (VHCF) range for two kinds of alloys used very largely in automotive engine components. Based on the test results and analyses presented in this paper, practical applications are being actually carried out in the automotive industry essentially in France.

Originality/value: Ultrasonic fatigue damage (VHCF $>10^9$) in VHCF is originally different from classical fatigue (up to 10^6) by typical internal fish eye formation. Additionally, fatigue crack of all the fractured specimens for the 2-AS5U3G-Y35 specimens initiated at the surface of the specimens. Fatigue fracture surfaces of AISI52100 steel specimens show a typical "scorpion-shaped" formation, which was considerably different from the fatigue fracture specimen subjected to axial cyclic loading, which exhibited the "fish-eye" formation.

Keywords: Damage mechanisms; Ultrasonic fatigue; Cyclic torsion; Very high cycle regime; SEM

Reference to this paper should be given in the following way:

E. Bayraktar, H. Xue, F. Ayari, C. Bathias, Torsional fatigue behaviour and damage mechanisms in the very high cycle regime, Archives of Materials Science and Engineering 43/2 (2010) 77-86.

PROPERTIES

1. Introduction

The fatigue of materials in the very high cycles (VHCF) regime (>10^7 cycles) has been studied in the past 20 years to understand the fatigue damage mechanism of mechanical parts subjected to very high vibrations [1-4]. Recent works using ultrasonic fatigue testing devices (20-30 kHz) have shown that many materials, including some steel, aluminium alloy and titanium alloys, intermetallics composites, etc., exhibit a sharp decrease in the fatigue strength between the fatigue lives of 10^6 and 10^9 cycles [1-9]. Hence, it is important to investigate the fatigue behaviour of materials in this very high cycle regime. Several fatigue investigations in the VHCF range of the metallic materials have shown that damage initiated in the very high cycle fatigue ranges well below the traditional fatigue limit, which was predicted by the "classical Wöhler S-N curve" as alluded to in Ref 1-39.

A long standing understanding of fatigue damage in the VHCF range was that the internal defects were initiated from non-metallic inclusions. However, recent research has hypothesized a defect formation mechanism that is correlated to fatigue threshold values in every stage of the fatigue evolution. There are also different hypotheses for the evolution of the S-N curves up to the VHCF range. For example, Nishijiama [1] and Murakami [2] proposed the variation of the S-N curve by different steps, while Bathias [3] and Sakai [4, 5] demonstrated that there is no fatigue limit in the VHCF range. This hypothesis was further supported by a well-known scientific paper of Bathias [3]. Recently, Bayraktar et al. [10] suggested that the origin of the internal damage was due to the slip bands and the nature of the microstructure in addition to inclusions and pores leading to the formation of the fish eye. For example, two different phases of the microstructure, which have different mechanical properties, cause different behaviour in the same solicitation. They also provided different interpretations for the damage due to different internal, subsurface and surface crack initiation types in the VHCF range. These ideas were discussed in the Paris conference held in 1998 in regards to "Euromech-382".

The ultrasonic fatigue testing method is not restricted to cyclic axial loading. Many present engineering components used in modern technology work under combined torsion and axial loading, and the cyclic combined loading can result in fatigue fracture after a very long life fatigue regime. However, only a few research groups have carried out ultrasonic torsional fatigue tests in the VHCF regime to explain the fatigue properties of materials under ultrasonic torsional cyclic loading [11, 13, 14, 15, 34, 36, 38, 39].

To the best of our knowledge, there is insufficient evidence in the literature on the damage mechanisms under ultrasonic torsional fatigue in the VHCF range. Knowledge of the behaviour of materials under cyclic torsion is of great interest, since loading of many mechanical components is under cyclic torsion rather than cyclic tension-compression. Lukas et al. [32] have shown the main differences in damage between low and high cycle fatigue. They have shown that plastic deformation in the VHCF range is restricted to only one or two grains, whereas other grains may stay in a purely elastic range. Plasticity also occurs mainly in surface grains, which are less constrained, compared to the interior grains. In this study, we evaluated the torsional fatigue properties of cast aluminium 2-AS5U3G-Y35 and AISI52100 steel, which are important alloys used in automotive engine components. These components are known to be subjected to low amplitude, high cycle, high frequency cyclic loading in working service. Thus, it is important to examine fatigue behaviour and the damage mechanism of these alloys in the very high cycle regime. Bayraktar et al [13, 34, 36, 37] have investigated in detail the VHC- fatigue behaviour of different kinds of automotive alloys and interpreted damage mechanisms in longitudinal loading conditions. Thus, the present paper focuses only on pure torsional fatigue testing and the damage mechanisms in the VHCF range.
Structural mechanical components subjected to high frequency vibrations, such as those used in rotating parts in engines, are usually designed with a lifetime failure-free criterion for a very large endurance limit. Fatigue data in longitudinal loading are insufficient for assessing the VHC- fatigue limit of the components that are subjected to torsional cyclic loading as indicated by Stanzl - Tschegg et al [6]. In rotating components, fatigue failure occurs after a long life subjected to combined bending and torsional strains at very high frequencies. Since 1993, Stanzl-Tschegg and Mayer [6, 8, 11, 27, 38] have designed and constructed an ultrasonic torsional fatigue test system at a frequency of 21 kHz to investigate torsional fatigue behaviour of alloys. Although much evidence exists for the fatigue behaviour under axial loading in the VHCF range, insufficient data can be found for torsional loading in the literature [8, 13, 27, 31, 34-39].

All torsional fatigue tests were done on the new torsional fatigue testing machine at a high frequency of 20 kHz corresponding to fixed numbers of cycles of up to 10^{10} cycles. These tests were developed in the context of two industrial projects [13, 18]. This torsional testing machine was constructed differently from the machine of Stanzl-Tschegg et al. [6, 8], as explained in the following section.

2. Experimental study

2.1. Testing material

The materials used in this study were cast aluminium 2-AS5U3G-Y35 and high strength steel AISI 52100. Their nominal compositions and mechanical properties are given in Tables 1 and 2, respectively. Both of the materials were prepared by industrial partners and all of the specimens have been polished to obtain the same surface conditions (with emery paper up to 2000).
Fig. 1 shows the typical microstructures of the materials used in this study. AISI52100 steel was essentially martensitic steel and after a special tempering treatment it had a fine microstructure, with very fine ferrite being evenly distributed in the microstructure, and there were very elongated inclusions of predominantly MnS distributed in the microstructure with very high aspect ratios, AR ($AR=d_{length}/d_{width}$) They can vary from 7 up to 15. Aluminium has a typical eutectic structure with primarily dendritic cells (aluminium matrix, black) composed of eutectic silicon (white) particles and Fe- and /or Mg-bearing intermetallics in the inter- dendrite region [10].

Table 1.
Chemical composition of Al and AISI52100 steel (wt %)

Material	C	Mn	P	S	Si	Fe	Mg	Ni	Cr	Cu	Mo
2-AS5U3G-Y35	-	0.32	-	-	5.3	0.57	0.36	-	-	3.15	-
AISI52100	1.03	0.339	0.012	0.008	0.242	-	-	0.147	1.461	-	0.032

Table 2.
Mechanical properties of aluminium and AISI52100 steel

Material	E(GPa)	$\rho(g/cm^3)$	A(%)	$\sigma_{0,2\%}$(MPa)	UTS(MPa)	HV30
2-AS5U3G-Y35	72	2700	1	182	222	99
AISI52100	210	7860	-	1158	2300	780

2.2. Testing and measurement systems

We designed an ultrasonic torsion fatigue system to determine the torsion fatigue limit of the alloy up to 10^{10} cycles [8]. The main component of the ultrasonic system was a piezoelectric transducer, which converted an electrical signal at a frequency of 20 kHz into a mechanical displacement at the same frequency. Two horns were attached to the transducer; the first one amplified the longitudinal mechanical displacement, while the second amplified the torsional angular displacement (Fig. 2). The second horn was connected at the end of the first horn to transform the longitudinal displacement into torsional displacement. A torsion fatigue specimen was designed to run in the same resonance with the system and was directly attached at the end of the second horn. The specimens were designed so that the maximum strain was located in the gage section as illustrated in Fig. 2.

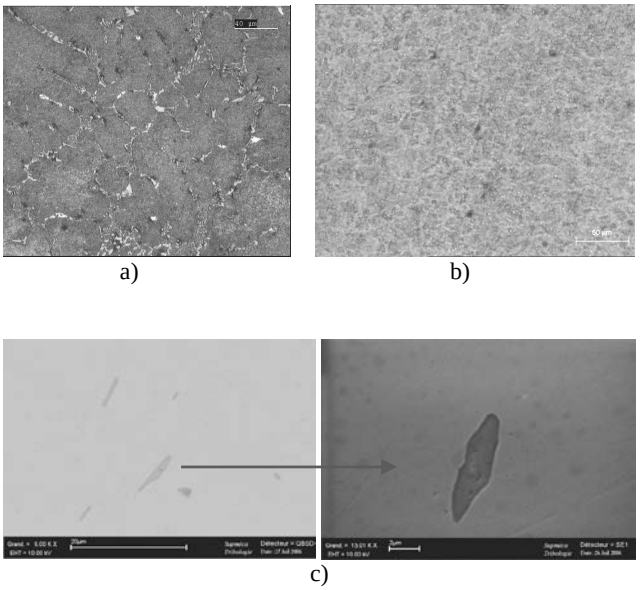

Fig. 1. Microstructure of test alloys a) 2-AS5U3G6Y35; b) AISI52100; c) slender shape inclusions found in AISI52100

In this study, all of the tests were carried out at a stress ratio of R= –1. Before each test, the strain of specimen in the gage length was calibrated with a strain gage bonded to the gage section. Under the nominal elastic conditions, a linear relationship was constructed between input displacement and the strain in the gage section for the calibration of the system. The system calibration result is shown in Fig. 3. The automatic test control software continuously recorded the displacement and controlled the output of the power supply to control the magnitude of the strain in the specimen. This was the basic working principle of the torsional fatigue machine used in this study. More technical details related to the torsional fatigue system can be found elsewhere [13, 18, 34].

2.3. Geometry of the specimens

The two different specimen geometries for the two alloys used in the ultrasonic torsional fatigue tests are shown in Fig. 4a. A torsion specimen for each alloy was designed to run in resonance with the system, and its dimension was determined by analytical or numerical methods (ANSYS) depending of the material properties such as density, Elastic modulus, etc. [7, 9] and have calculated the evolution of the displacement and stress in the specimens as given in the Fig. 4b. It shows that torsional shear loading occurs in the centre of the specimen with the maximum amplitude. The maximum stress is always at the centre of the specimen where the displacement is zero. The ultrasonic torsional fatigue specimens were considerably smaller than the specimens used for tension-compression fatigue testing, as the wavelength of shear waves was shorter.

2.4. Design of ultrasonic fatigue test and implementation

Torsional fatigue tests were done under ambient conditions using the ultrasonic torsional fatigue machine [13, 18] with the stress ratio R = -1. In this system, the specimen was excited to torsion resonance vibration at the ultrasonic frequency of 20 kHz. This led to torsional shear loading with the maximum amplitude occurring in the centre of the specimen. The entire of the specimens were cooled homogenously with dry air during fatigue testing to decrease the temperature rise caused by internal friction of the material. Failure of the specimens was detected by monitoring the resonant frequency, which enabled the automatic operation of the experiments.

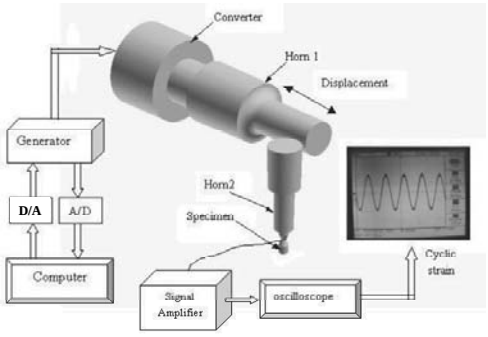

a)

b)

Fig. 2. a). System design of torsional fatigue vibration system developed in CNAM and b). Testing device in laboratory scale [13, 18, 34]

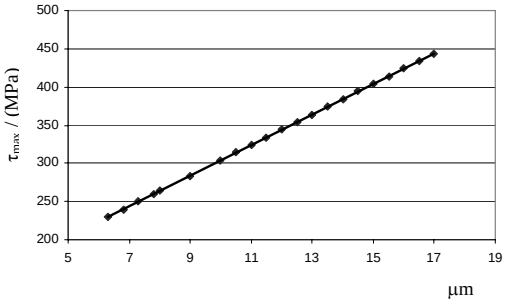

Fig. 3. System calibrating result in cyclic torsion

This automation caused the tests to stop automatically when the specimen failed before attaining 10^{10} cycles. The staircase method was used to obtain accurate values of the fatigue limit stress for both kinds of metallic alloys corresponding to the fixed number of cycles, up to 10^{10} cycles. The results obtained for were compared to those of the conventional torsional fatigue test machine operated at 35 Hz to observe if there is a discrepancy in results due to frequency effects between two experiments.

Fatigue crack initiation, the microstructure and short cracks in the fatigue specimens were examined using both optical and scanning electron microscopes (SEM). The chemical compositions at the crack initiation site were analysed by spectrometry (EDS).

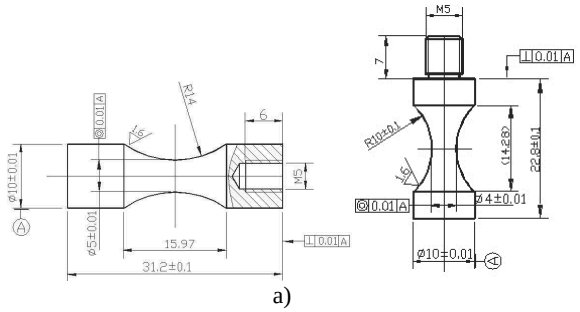

a)

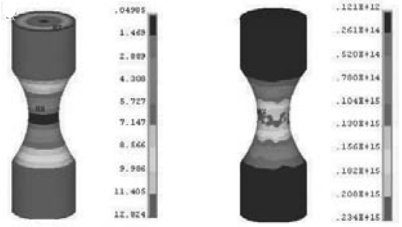

b)

Fig. 4. a) Dimension of ultrasonic torsion fatigue specimens and b) Evolution of the displacement and stress in the torsion specimen given by numerical methods (ANSYS)

3. Experimental fatigue test results

The fatigue properties of the alloys under constant amplitude loading were examined. The stress-life (S-N) curves for two materials, 2-AS5U3G-Y35 and AISI52100, are shown respectively in Fig. 5a and Fig. 5b. In Fig. 5a, solid markers represent data obtained when the specimens were tested at 35 Hz (carried out in RENAULT-Paris), while open markers represent data for 20 kHz (carried out in CNAM-Paris) test frequencies in the ultrasonic torsion fatigue test machine. In the same way, data, represented in Fig. 5b, have been obtained at 35 Hz (solid circle markers) and for 20 kHz (solid rectangular markers) test frequencies in the ultrasonic torsion fatigue test machine. The S-N curves show that fatigue failure of these alloys could occur up to the 10^{10} cycles. For the specimens of cast aluminium, fatigue life increased with decreasing stress amplitude in the life range of 10^4-10^7 cycles, and fatigue fracture occurred even beyond 10^7 cycles, although the slope of the S-N curve decreased slightly (Fig. 5a). For AISI52100, a horizontal asymptote could not be drawn between 10^7 and 10^{10} cycles, and the scatter of the data was very high (Fig. 5b). This effect was due to the high strength of the steel, which had fine microstructures with too fine ferrite being evenly distributed in the microstructure, and there were very elongated inclusions of mostly MnS distributed in the microstructure with very high aspect ratios ($AR=d_{length}/d_{width}$) that are variables from 7 to 15). This situation could introduce these dispersions. In any case; for the metallurgical reasons and/or the density and the probability of the distribution of the inclusions from the specimen to specimen, the S-N curves of these alloys show systematically and continuously decreasing up to the gigacycle range. Although these defined by means of statistical

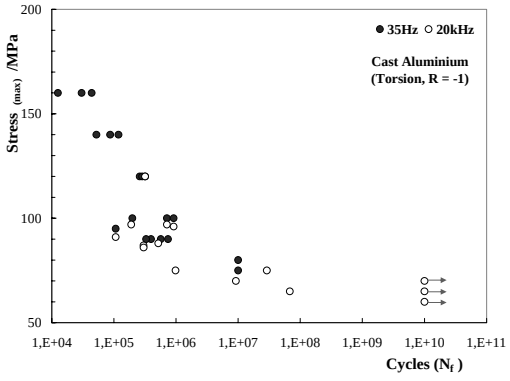

a)

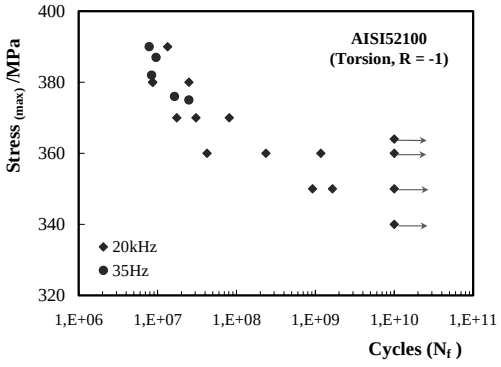

Fig. 5. a) Torsion fatigue test results (*R*=-1), 2-AS5U3GY35 and b) AISI52100

analysis between 10^6 and 10^7 cycles cannot guarantee a safe design of the components subjected to very high frequencies.

4. Discussion

4.1. Fracture surface analysis

In general, inspection of the fractured specimens shows the well-known fatigue mechanisms in the torsion fatigue tests [10-12]. Shear crack nucleation was followed by crack growth on the planes of maximum principal stress amplitude. Typical crack patterns observed at the surfaces of the specimens of cast aluminium are shown in Fig. 6a and 6b. We note that a small crack was initiated on one of the planes where shear stress was at a maximum and that it can propagate up to a length of several hundred microns before branching, which propagated on one of the planes of maximum normal stress. However, for the AISI52100 (as will be seen later in the Fig. 8-10) and some of the aluminium specimens, the crack growth was developed only on the planes of maximum normal stress (i.e., on a plane of 45º).

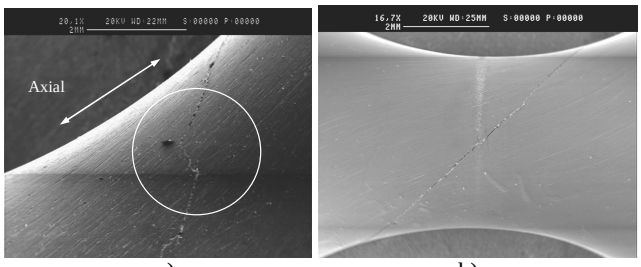

a) b)

Fig. 6. a) Torsion surface crack patterns in the failed steel specimen, small crack initiated on the plane of maximum shear and propagated in 45° plane and b) crack growth occured only at 45° plane

Additionally, crack initiation and propagation in the failed specimens were observed (Fig. from 7a) to 7c)). Fatigue crack of all the fractured specimens for cast aluminium regularly initiated at the surface of the specimens [13, 34]. Fig. 7 shows a typical torsion fatigue fracture surface of cast aluminium, at an applied maximum stress level of 70 MPa. The fatigue crack growth plane reveals a spiral 45° fracture plane, and fatigue initiation began from the surface of the specimen and show regularly a propagation stage Fig. 7c).

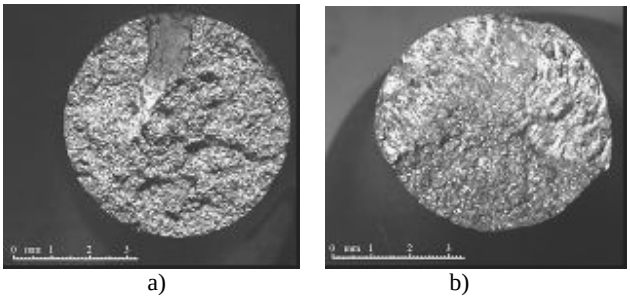

a) b)

Fig. 7. a) Fracture surfaces of 2-AS5U3G-Y35 specimens produced by ultrasonic cyclic torsion (τ_{max} = 70MPa, R =-1, $N_f = 9.5x10^7$) and b) Static fracture occurred in the centre area (both of the pictures were taken in macroscopic scale)

This idea given here and in [13, 34, 36] is new, because in literature, a common idea particularly in [3-6, 24, 27, 33, 40] says that fatigue damage in gigacycle regime is characterised basically by initiation stage, it means that the time elapsed up to the first appearance of the crack is important and the propagation life is too short and not important at all. More important idea has been given by P. Paris et al. [40] in the fatigue conference-Kyoto (VHCF -3). P. Paris et al. has established the relationship of effective stress intensity, elastic modulus and Burgers vector on Fatigue Crack Growth as associated with “Fish Eye” in gigacycle regime. They explained that there is quasi no propagation stage and/or is too short because their formula shown that more than 90% of the total fatigue life is determined by initiation stage. However, our experimental results [13, 34, 36] and this paper show opposite results regarding to the common idea given in the

literature. It means that there is an important propagation life in gigacycle regime and the fracture surfaces taken in SEM of the tested specimens verify this idea very clearly in our experimental conditions. The propagation stage is important in gigacycle fatigue regime in the axial and torsional solicitation (Fig. 7c and later Fig. 9-II).

Typical detail torsional fatigue fracture surfaces of AISI52100 and typical crack patterns observed at the surface are shown in Fig. 8-I and II. These pictures clearly show the cracking on the longitudinal plane (i.e., maximum shear plane), with the final facture occurring in a spiral shape on a 45º plane (maximum principal stress plane). Although the failure crack may become visible on the

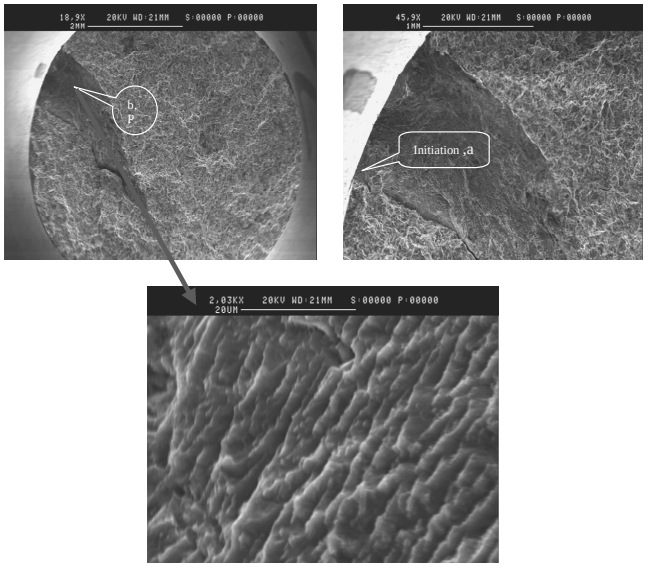

Fig. 7c). Fracture surfaces of Al specimens taken from SEM, ultrasonic cyclic torsion (stable crack growth and crack initiation and crack propagation zones), (τ_{max} = 70MPa, R =-1, $N_f = 9.5x10^7$)

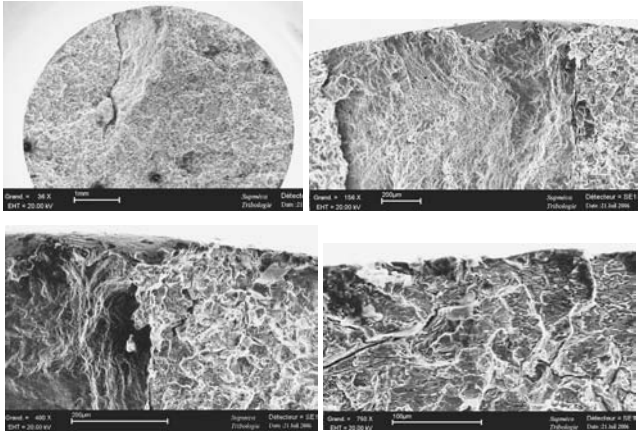

Fig. 7d). Fracture surface taken from SEM, idem for the specimen given in 7a), b), c) (τ_{max} = 70MPa, R =-1, $N_f = 5x10^7$)

maximum principal stress plane at 45º, the fatigue damage mechanism was shear. As expected, the fatigue crack initiated from the surface at higher stress amplitudes, but there was a transition of crack initiation from surface to subsurface and inside of the specimen respectively. Fatigue crack initiation of most of the specimens was from subsurface and inside inclusions for the specimen of AISI52100, as shown in Fig. 8-I and II. A dark area near the crack origin was not regular as observed in the specimens tested in longitudinal fatigue solicitation in gigacycle regime. EDS analysis carried out at and near the failure origin were non metallic inclusions mainly in elongated form and major ones were MnS inclusions.

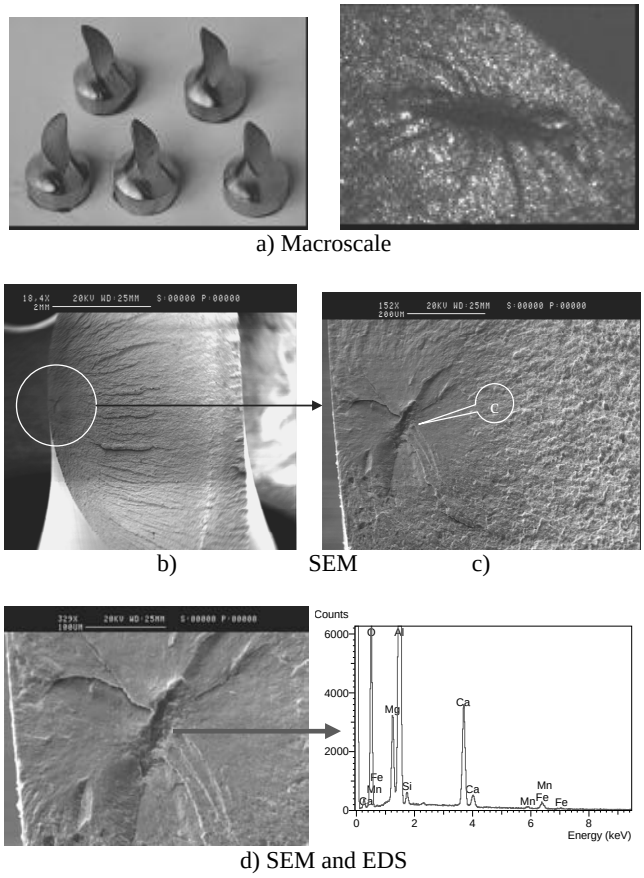

Fig. 8-I. Fatigue fracture surfaces of AISI52100 produced by ultrasonic cyclic torsion; a) fractured specimens and appearance of "scorpion or spider-shaped form"; b) fracture surfaces showing fatigue crack initiation from the inside inclusion; c-d) detail of "scorpion or spider form" and inclusion; (τ_{max}=370MPa; N_f=3.06x10^7 cycles)

The subsurface and even inside crack initiation was observed in most fatigue-tested samples for AISI52100 with the fatigue life between 10^7 and 10^9 cycles. The fatigue fracture surfaces regularly showed a "scorpion or spider-shaped" formation, which was considerably different from the fatigue fracture specimen subjected to axial cyclic loading, which exhibited mostly fish-eye shaped formations. Even the temperature is controlled regularly in

all parts of the specimen during the test, the temperature measurements showed that maximum temperature at the centre of the specimen has arrived at 70°C and 120°C.

The dark zone around the inclusion was very small, not circular in shape but elliptical. The area of the dark zone was also too small or not always existing regarding to that of the fatigue fracture surfaces subjected to the axial cyclic loading [10, 17-19]. It is likely that the formation of “scorpion or spider-shaped” formations in AISI52100 was due to the major role of shear stresses on the damage mechanisms under torsional cyclic loading in the gigacycle regime and the effect of the elongated form of the inclusions plays also a role on the scorpion or spider-shaped” formation.

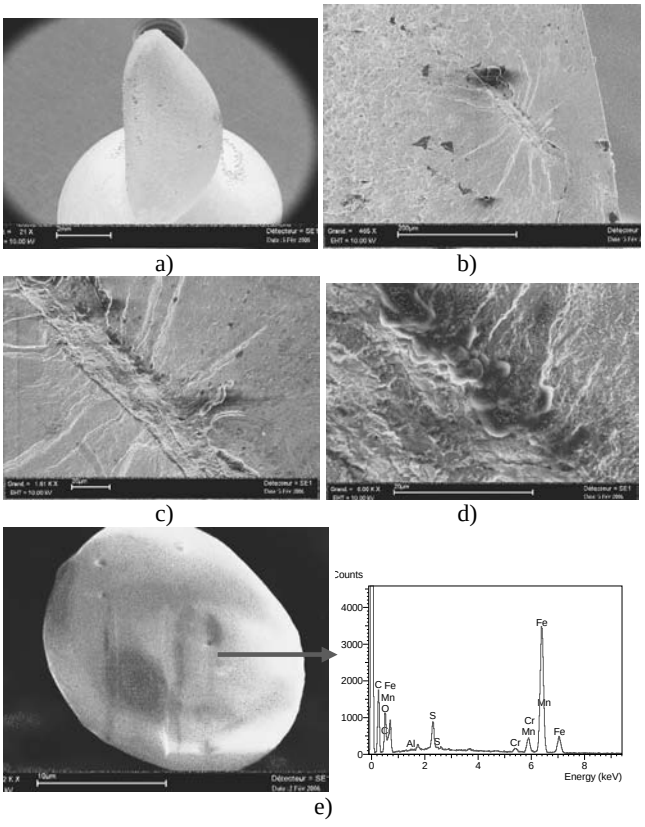

Fig. 8-II. a) Fracture surface of AISI52100 produced by ultrasonic cyclic torsion, which was cycled at 375 MPa and failed at $3.5x10^8$ cycles, b-d) “Scorpion shaped” formation at subsurface and detail of stable crack growth and crack initiation zones with plastic zone, e) typical inclusion and EDS analysis in AISI52100

Additionally, Fig. 9-I and II show a typical fracture surface observed in the gigacycle regime. In the centre of the “scorpion or spider” formation was an inclusion with fine granular elongated facets around it.

Here, a propagation stage has been clearly observed in an important part of the fracture surface, just around the scorpion or spider formation. There is no dark area and or no smooth fracture surface around the scorpion or spider-shaped” formation. In the literature, the formation of "fish-eye" is due to internal vacuum environment. Crack propagation in vacuum create smooth fracture surface, so the internal crack propagation area is clearly distinguished from that after the crack reaches the surface. This case is not found in this study and studies given in [13, 34, 36].

In summary, the "scorpion or spider-shaped" formation is due to the major role of shear stresses on the damage mechanisms under torsional cyclic loading in the gigacycle regime and also likely to depend on the shape of the elongated inclusion; most of the fracture surfaces verify that there is a slender shape of the MnS inclusion.

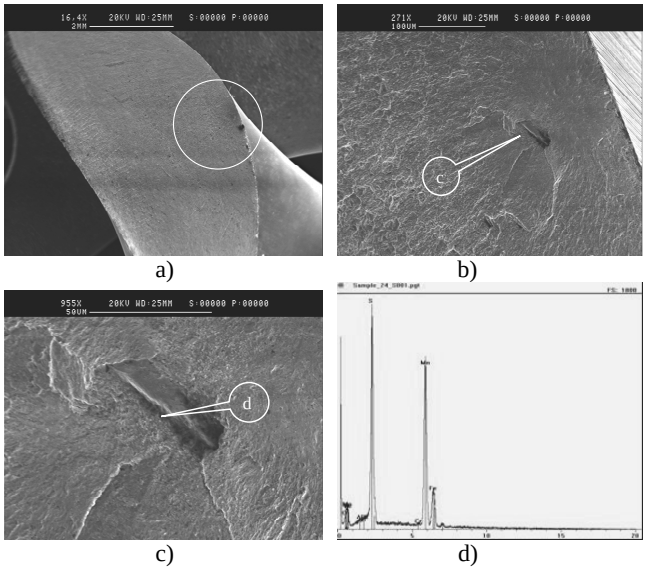

Fig. 9-I. Fatigue crack initiation from the inside a) fatigue fracture surface; b) stable crack propagation, c) inside fatigue initiation and EDS analysis d), (τ_{max} = 380MPa; N_f =$3.5x10^8$)

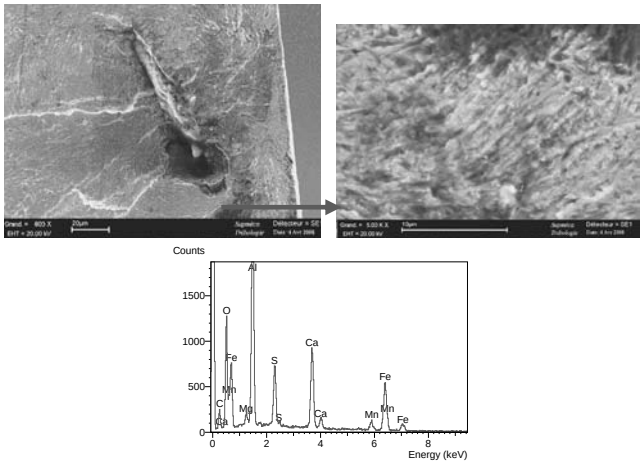

Fig. 9-II. Fatigue crack initiation and propagation stage and EDS analysis for the given specimen (τ_{max} = 350MPa, N_f =$9.45x10^8$ cycles)

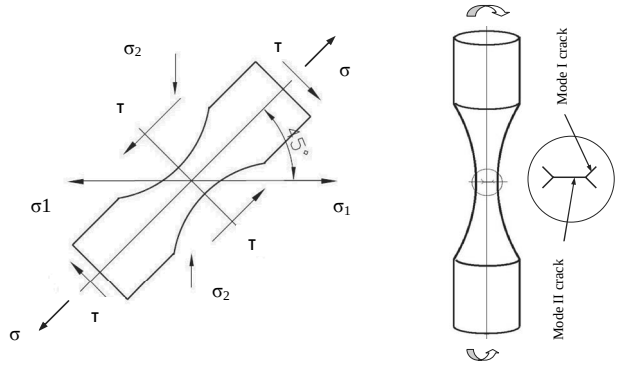

a) b)

Fig. 10. a) Schematic presentation of the normal and shear stresses in torsion fatigue specimen tested in the present paper and b) Schematic presentation of fatigue crack modes under torsional fatigue loading studied in the present paper

The angle of the diagonal face was always 45° with respect to the loading axis. This type of crack initiation was true of most cases of fatigue fracture in the gigacycle regime.

4.2. Mechanism of fatigue crack initiation

The position of the normal and shear stresses is shown in Fig. 10 for the case where the specimen was subjected to torsion cycle loading. Both tensile and compressive stresses were at 45° to the specimen axis and remained mutually perpendicular. One shear stress component was parallel to the specimen axis, while the other was perpendicular. Under a cyclic torsional load, fatigue cracks initiated from the surface of the specimen where the shear stress valuess arrived the highest levels. When the fatigue crack initiated, the local stress increased, different states of stress were formed around the fatigue crack initiation, and local tensile stress on the 45° plane then exceeded the tensile strength of the alloys before the local shear stress exceeded the shear strength of the alloy. Thus, the fracture took place normal to the 45° tensile plane, producing a typical torsional fracture surface as shown in Fig. 10a.

As previously observed, when smooth specimens are subjected to torsional fatigue loading, crack initiation proceeded to Mode II [20-23] (Fig. 10b). This means that crack initiation occurred on the planes where the shear stress amplitude was largest. The early stages of the crack propagation on the specimen surface would also follow Mode II [20]. When the shear crack reached a threshold value, which was a function of the material and number of cycles to failure [23], crack branching would occur, and the crack would propagate in the same direction.

We note that, for the cast aluminium 2-AS5U3G-Y35 specimens subjected to torsional cyclic loading, crack initiation was always Mode II. On the contrary, in some particular situations, e.g., for failed specimens with lower fatigue lives, both crack initiation and propagation followed Mode I. For AISI52100 specimens, inclusions existed in the microstructure, which played an important role in the crack initiation type.

In summary, the results of the present study indicate that fatigue cracks also initiate from subsurface and inside inclusions for the high strength steel in the VHCF range by the formation of “scorpion or spider shapes” due to shear effect. This situation results in local plastic deformation around an inclusion. In comparison to the high cycle fatigue fractured specimens subjected to axial cyclic loading, in torsional loading, the fatigue crack initiation was always from the subsurface or inside of the specimen in the VHCF range, with a special “scorpion or spider form” occurring due to the maximum shear stress at the surface of the specimen, but not from the inside of the specimen.

4.3. Mechanism of fatigue crack propagation

For the cast aluminium 2-AS5U3G-Y35 specimen, fatigue cracks initiated from the centre of the specimen where it was subjected to the maximum shear stress under cyclic torsional loading. When fatigue crack initiation occurs, the local stress increases, and different states of stress form around the initiation site. The local tensile stress on the 45° plane will largely exceed the tensile strength of the alloys before the local shear stress reaches the shear strength of the alloy. This effect is similar to that observed for the other sample. Thus, fracture occurred normal to the 45° tensile plane, thus producing a typical torsional fracture surface, as shown in Fig. 6 and 10.

When the fatigue crack initiated from a subsurface inclusion in the AISI52100 steel, micro-cracks would grow around the inclusion, thus forming a facet area (Fig. 8 and Fig. 9). Hence, when the fatigue crack reached the specimen surface, the fatigue crack would propagate as surface cracks. When the micro-cracks propagated to the surface of specimen, crack growth occurred in the cyclic tension stress plane at 45° to the axial direction. In this case, shear cracks did not occur. In other words, fracture of the specimen initiated from a subsurface inclusion revealing a completely 45° fracture surface, as shown in Fig. 6b. Examinations of the broken specimen showed that the crack always propagated in plane at 45° to the axial direction.

Fatigue test results show that the fracture surface contained fatigue striations. The crack propagations were oriented at approximately 45° to the axis of specimen, indicating that the final fracture was the origin of the tensile stress normal to the 45° plane. It is therefore not the shear stress that caused an overload failure.

In some of aluminium specimens tested under low cyclic stress, smaller shear steps are very evident on the spiral 45° fracture plane, although the big shear steps were not present. In addition, many micro-cracks were observed around the principle crack in a several fatigue fracture surfaces. This tendency indicates that fatigue crack initiation and propagation occur on one of the planes of maximum shear stress. Moreover, while crack branching occurred, only the principal crack produced the final failure of specimen.

In contrast, secondary cracks can be easily found on the fracture surfaces. The cleavage-like fracture surface occurred in the final overload region. However, for the AISI 52100 specimens, where cracks initiated from subsurface or inside inclusions, the above crack propagation characteristics were not observed regularly but some of the specimens have shown clearly important crack propagation characteristics.

5. Conclusions

We investigated torsional fatigue tests in the VHCF range for two kinds of alloys used in automotive engine components. Based on the test results and analyses presented in this paper, the following conclusions can be made:

- Fatigue crack of all the fractured specimens for the 2-AS5U3G-Y35 specimens initiated at the surface of the specimens. Fatigue fracture surfaces of AISI52100 steel specimens show a typical "scorpion-shaped" formation, which was considerably different from the fatigue fracture specimen subjected to axial cyclic loading, which exhibited the "fish-eye" formation. Fatigue cracks always initiated from the subsurface just beneath the specimen surface and never initiated from internal inclusion, although the specimen had very high cycle fatigue lifetimes. The formation of "scorpion or spider shapes" in the AISI52100 steel showed very clearly the major role of shear stress on the damage mechanisms under torsional cyclic loading in the VHCF range and also likely to depend on the shape of the elongated inclusion; most of the fracture surfaces verify that there is a slender shape of the MnS inclusion.
- The fatigue crack initiated from the surface of the specimen at higher stress amplitudes, but there was a transition of the crack initiation from the surface to the subsurface and even inside of the specimen in the gigacycle regime for the AISI 52100 steel due to an obvious inclusion in the microstructure, which was principally MnS.
- Damage mechanisms under torsional fatigue loading comprise two stages, i.e., crack initiation and crack propagation. This mechanism is contrary to the damage under axial loading, which exposed only a crack initiation mechanism in the VHCF range. - The crack propagation life is important for a solid specimen under cyclic torsion loading. This case is demonstrated by the many shear striations at fatigue fracture surface

Acknowledgements

The authors are grateful to the research managers of RENAULT-FRANCE and E. Bayraktar personally thanks to North western Polytechnical University, School of Aircraft Design Engineering, Xi'an China for their kind scientific collaboration with this project

References

[1] S. Nishijiama, K. Kanazawa, Stepwise S-N curve and fish-eye failure in gigacycle regime, Fatigue and Fracture of Engineering Materials and Structures 22 (1999) 601-607.

[2] Y. Murakami, Y. Takada, T. Toriyama, Super-long life tension-compression fatigue properties of quenched and tempered 0.46%C steel, International Journal of Forecasting 16 (1998) 661-667.

[3] C. Bathias, There is no infinite fatigue life in metallic materials, Fatigue and Fracture of Engineering Materials and Structures 22 (1999) 559-565.

[4] H.Q. Xue, E. Bayraktar, C. Bathias, Fatigue behaviour and energy dissipation of a nodular cast iron in ultrasonic fatigue loading, Journal of Achievements in Materials and Manufacturing Engineering 18/2 (2006) 251-254.

[5] T. Sakai, H. Hirano, T. Tomoto, A study on ultra long life fatigue characteristics in rotating bending for aluminium alloy with some surface treatments, Proceedings of the 3rd International Conference "Very High Cycle. Fatigue" VHCF-3, Kyoto, 2004, 585-592.

[6] S.E. Stanzl-Tschegg, H.R. Mayer, E.K. Tschegg, The influence of air humidity on near-threshold fatigue crack growth of 2024-T3 Al alloy, Materials Science and Engineering: A 147 (1991) 45-54.

[7] E. Bayraktar, H. Xue, C. Bathias, Damage mechanisms of Ti-Al inter-metallic in three point ultrasonic bending fatigue, Journal of Achievements in Materials and Manufacturing Engineering 24/1 (2007) 153-161.

[8] H. Mayer, M. Papakyriacou, B. Zettl, S.E. Stanzl-Tschegg, Influence of porosity on the fatigue limit of die cast magnesium and aluminium alloys, International Journal of Forecasting 25 (2003) 45-256.

[9] J.R. Morrissey, T. Nicholas, Fatigue strength of Ti-6Al-4V at very long lives, International Journal of Forecasting 27 (2005) 1608-1612.

[10] E. Bayraktar, M.G. Israel, C.O. Bathias, Failure mechanisms of automotive metallic alloys in very high cycle fatigue range International Journal of Forecasting 28 (2006) 1590-1602.

[11] J. Sieniawski and M. Motyka, Superplasticity in titanium alloys, Journal of Achievements in Materials and Manufacturing Engineering 24/1 (2007) 123-130

[12] M.J. Tan, X.J. Zhu, Dynamic recrystallisation in commercially pure titanium, Journal of Achievements in Materials and Manufacturing Engineering 18/2 (2006) 183-186.

[13] H. Xue, Explanation on gigacycle fatigue of materials in tension, bending and torsion loading, PhD thesis, CNAM, Paris-FRANCE, 2005.

[14] P. Davoli, A. Bernasconi, M. Filippini, Independence of the torsional fatigue limit upon a mean shear stress, International Journal of Forecasting 25 (2003) 471-480.

[15] D. Mcclaflin, A. Fatemi, Torsional deformation and fatigue hardened steel including mean stress and stress gradient effects, International Journal of Forecasting 26 (2004) 773-784.

[16] L.A. Dobrzański, E. Jonda, A. Polok, A. Klimpel, Comparison of the thermal fatigue surface layers of the X40CrMoV5-1 hot work tool steels laser alloyed, Journal of Achievements in Materials and Manufacturing Engineering 24/2 (2007) 135-138.

[17] H. Mughrabi, On the life-controlling microstructural fatigue mechanisms in ductile metals and alloys in the gigacycle regime, Fatigue and Fracture of Engineering Materials and Structures 22 (1999) 633-641.

[18] W. Pilarczyk, R. Nowosielski, M. Nowak, M. Kciuk, The structural changes of Al-Ti-Fe alloy during mechanical alloying process, Journal of Achievements in Materials and Manufacturing Engineering 29/2 (2008) 131-138.

[19] H. Mughrabi, Specific features and mechanisms of fatigue in the ultrahigh cycle regime, Proceedings of the 3rd International Conference "Very High Cycle Fatigue", Japan, Kyoto, 2004, 14-23.
[20] D. Socie, J. Bannantine, Bulk deformation fatigue damage models, Materials Science and Engineering A 103 (1988) 3-13.
[21] G. Marquis, D. Socie, Long-life torsion fatigue with normal mean stresses, Fatigue and Fracture of Engineering Materials and Structures 23 (2000) 293-300.
[22] L. Susmel, D. Taylor, A simplified approach to apply the theory of critical distances to notched components under torsional fatigue loading, International Journal of Forecasting 28 (2006) 417-430.
[23] C. Makabe, D. Socie, Crack growth mechanisms in precraked torsional fatigue specimens, Fatigue and Fracture of Engineering Materials and Structures 24 (2001) 607-615.
[24] H. Mayer, C. Ede, J.E. Allison, Influence of cyclic loads below endurance limit or threshold stress intensity on fatigue damage in cast aluminium alloy 319-T7, International Journal of Forecasting 27 (2005) 129-141.
[25] Q.Y. Wang, J.Y. Berand, C. Bathias, Gigacycle fatigue of ferrous alloys, Fatigue and Fracture of Engineering Materials and Structures 22/8 (1999) 667-672.
[26] C. Bathias, How and why the fatigue S-N curve does not approach a horizontal asymptote, International Journal of Forecasting 23/1 (2001) 143-151.
[27] H. Mayer, Ultrasonic torsion and tension - compression fatigue testing: Measuring principles and investigations on 2024-T351 aluminium alloy, International Journal of Forecasting 28 (2006) 1446-1455.
[28] M. Rojek, J. Stabik, S. Sokół, Fatigue and ultrasonic testing of e-g composites, Journal of Achievements in Materials and Manufacturing Engineering 20/1-2 (2007) 183-186.
[29] G. Chai, Fatigue behaviour of duplex phase alloys in the very high cycle regime, Proceedings of the 3rd International Conference "Very High Cycle Fatigue", Japan, Kyoto, 2004, 374-381.
[30] N. Takashi, O. Hiroyuki, Characteristics of initial fatigue crack propagation process of Ti-6Al-4V in very high cycle fatigue, Proceedings of the 3rd International Conference "Very High Cycle Fatigue", Japan, Kyoto, 2004, 201-208.
[31] M. Papakyriacou, H. Mayer, C. Pypen, H. Plenk, S. Stanzl-Tschegg, Effects of surface treatments on high cycle corrosion fatigue of metallic implant materials, International Journal of Forecasting 22 (200) 873-886.
[32] P. Lukas, L. Kunz, Specific features of high-cycle and ultra-high-cycle fatigue, Fatigue and Fracture of Engineering Materials and Structures 25 (2002) 747-53.
[33] H. Mayer, M. Papakyriacou, B. Zettl, Endurance limit and threshold stress intensity of die cast magnesium and aluminium alloys at elevated temperatures, International Journal of Forecasting 27 (2005) 1076-1088.
[34] H.Q. Xue, E. Bayraktar, I. Marines-Garcia, C. Bathias, Torsional fatigue behaviour in gigacycle regime and damage mechanism of the perlitic steel, Journal of Achievements in Materials and Manufacturing Engineering 31/2 (2008) 391-397.
[35] Y. Murakami, H. Matsunaga, The effect of hydrogen on fatigue properties of steels used for fuel cell system, International Journal of Forecasting 28 (2006) 1509–1520.
[36] E. Bayraktar, R. Mora, I-M. Garcia, C. Bathias, Heat treatment, surface roughness and corrosion effects on the damage mechanism of mechanical components in the very high cycle fatigue regime, International Journal of Fatigue 1/10 (2009) 1532-1540.
[37] H. Xue, D. Wagner, N. Ranc, E. Bayraktar, Thermographic analysis in ultrasonic fatigue tests, Fatigue and Fracture of Engineering Materials and Structures 29 (2006) 573-580.
[38] D. Renowicz, S.J. Skrzypek, Crack initiation and propagation in Fe-Al matrix, Journal of Achievements in Materials and Manufacturing Engineering 22/1 (2007) 37-40.